

Hysteretic Dynamics of Domain Walls at Finite Temperatures

T. Nattermann,¹ V. Pokrovsky,^{2,3} and V. M. Vinokur⁴

¹*Institut für Theoretische Physik, Universität zu Köln, D-50937 Köln, Germany*

²*Department of Physics, Texas A&M University, College Station, Texas 77843-4242*

³*Landau Institute for Theoretical Physics, Chernogolovka, Moscow District, 142432, Russia*

⁴*Argonne National Laboratory, Argonne, Illinois 60439*

(Received 22 September 2000; published 22 October 2001)

Theory of domain wall motion in a random medium is extended to the case when the driving field is below the zero-temperature depinning threshold and the creep of the domain wall is induced by thermal fluctuations. Subject to an ac drive, the domain wall starts to move when the driving force exceeds an effective threshold which is temperature and frequency dependent. Similar to the case of zero temperature, the hysteresis loop displays three dynamical phase transitions at increasing ac field amplitude h_0 . The phase diagram in the 3D phase space of temperature, driving force amplitude, and frequency is investigated.

DOI: 10.1103/PhysRevLett.87.197005

PACS numbers: 74.60.Ge

Pinning dominated driven dynamics of elastic media in random environment is a paradigm for a vast diversity of physical systems. Examples include vortices in type II superconductors, charge density waves (CDW) in solids, stripe phases, Wigner crystals, dislocations in crystals, domain walls in magnets, and many others [1]. Having appeared first in the context of dislocation dynamics [2], the scaling theory of glassy dynamic state of random elastic media came to fruition in the context of CDW [3] and vortex lattices in high temperature superconductors [3,4], and enjoyed an impressive success in explaining a wealth of phenomenology of the low temperature vortex state [5]. A closely related subject is the zero-temperature depinning transition first studied for CDWs [6,7] and domain walls [8,9]. Despite the significant recent progress, several key questions specific to glassy dynamics are yet poorly understood. One of such fundamental key issues, although known and extensively studied for more than 100 years in magnets, is hysteresis of interfaces subject to the applied ac drive and related aging and memory effects. A quest for urgent progress in understanding hysteretic behavior of magnetic domain walls is motivated also by emerging technological nanoscale magnetic systems whose ac properties are controlled by the hysteretic dynamics of interfaces.

A step towards theoretical description of hysteretic behavior of disordered interfaces has been undertaken in [10], where the cyclic motion of the domain wall at zero temperature under the ac field was investigated and the resulting magnetization hysteretic loop was described. A finite temperature may change drastically the interface dynamics: thermally activated creep motion becomes possible at any small drive.

In this Letter we develop a unified description of thermally activated and overthreshold domain wall dynamics in *impure* magnets. We demonstrate that at finite temperatures new scales of length, activation energy, and force appear leading to emergence of a new, temperature- and

frequency-dependent threshold field in the case of ac drive. The latter is the first in a series of dynamical phase transitions. To be specific, we will speak on magnetic domain walls. Accordingly, we will be using either of the terms “force” or “field” equivalently.

Finite temperature dc dynamics.—The essential of the zero-temperature dynamic behavior of an elastic medium in a random environment is the existence of the finite threshold depinning force h_p , separating immobile at $h < h_p$ and sliding at $h > h_p$ states of the system. Near the threshold the sliding velocity v shows a critical behavior [6–9] $v \sim (h - h_p)^\beta$. At finite temperatures and $h \ll h_p$ thermally activated drift motion controlled by the static rugged energy landscape occurs. The latter is governed by the interface free energy

$$\mathcal{H} = \int d^D x \left\{ \frac{1}{2} \Gamma (\nabla Z)^2 + V(\mathbf{x}, Z) - hZ(\mathbf{x}) \right\}, \quad (1)$$

where Γ is the interface stiffness, h is the external driving force, and $V(\mathbf{x}, Z)$ is the random impurity potential. D -dimensional vector \mathbf{x} is the coordinate along the interface, and Z is the coordinate of the transverse interface displacement. In the following we assume that the disorder average of the random potential vanishes. There are two different types of impurities, random bond (RB) and random field (RF) type in terms of magnetic models. The RB potential obeys the Gaussian statistics with

$$\overline{V_{\text{RB}}(\mathbf{x}, Z) V_{\text{RB}}(\mathbf{0}, 0)} = v^2 l^{D+1} \delta(\mathbf{x}) \delta(Z), \quad (2)$$

where $v^2 = v_0^2 c$. v_0 , c , and l denote the strength, the concentration, and the correlation length of the impurity potential. In the RF case $V_{\text{RF}}(\mathbf{x}, Z) = \int_0^Z h(\mathbf{x}, Z') dZ'$ where the RF $h(\mathbf{x}, Z)$ has properties similar to $V_{\text{RB}}(\mathbf{x}, Z)$.

The static interface in a random environment becomes rough. Its roughness obeys the scaling law [11]:

$$w^2(L) = \overline{[Z(\mathbf{x}) - Z(\mathbf{0})]^2} \approx l^2 \left(\frac{L}{L_p} \right)^{2\zeta}; \quad L = |\mathbf{x}|, \quad (3)$$

where the roughness exponent is $\zeta = \frac{4-D}{3}$ for RF, and $\zeta \approx 0.2083(4-D)$ for $4-D \ll 1$ and $\zeta = 2/3$ for $D = 2$, for RB impurities, respectively [11,12]. The rough configuration develops over length scales $L \geq L_p$, where the Larkin length L_p is a distance at which a typical fluctuation of the pinning forces, balanced by elastic forces, produces the transverse displacement $w \sim l$:

$$L_p \approx l(\Gamma/v)^{2/(4-D)}. \quad (4)$$

Note that the typical slopes $w(L)/L$ of the wall vanish for $L \gg L_p$ since $\zeta < 1$. The energy barrier which must be overcome to depin a segment of the wall with the linear size L is [2]

$$E_{B,0}(L) \approx T_p(L/L_p)^\chi; \quad \chi = D - 2 + 2\zeta. \quad (5)$$

Here $T_p \equiv E_{B,0}(L_p) \approx \Gamma l^2 L_p^{D-2}$ is a typical pinning energy on a scale L_p . At temperature $T > T_p$ the effective force necessary for depinning drops rapidly with the temperature [2]. In the presence of an external driving force h , the total energy barrier $E_B(L)$ becomes

$$E_B(L) \approx E_{B,0}(L) - hL^D w(L) = E_{B,0}(L) \left[1 - \left(\frac{L}{L_h} \right)^{2-\zeta} \right], \quad (6)$$

where $L_h \approx L_p(h_p/h)^{1/(2-\zeta)}$. Thermally activated creep motion at $h \ll h_p$ is controlled by the critical segments of size L_{opt} at which $E_B(L)$ reaches its maximum $E_{B,\text{max}}$: segments with $L < L_{\text{opt}}$ collapse, while segments of the lengths $L > L_{\text{opt}}$ expand and contribute to the motion. One finds $L_{\text{opt}} \approx \left(\frac{\chi}{D+\zeta} \right)^{1/(2-\zeta)} L_h$ giving [2]

$$E_{B,\text{max}} \approx T_p(h_p/h)^\mu, \quad \mu = \chi/(2-\zeta). \quad (7)$$

According to Middleton [13], in the vicinity of h_p the relevant pinning barriers should vanish as $(h - h_p)^\theta$ [14]. Replacing T_p by $\tilde{T}_p = T_p \left(\frac{h_p - h}{h_p} \right)^\theta$ in $E_{B,\text{max}}$ we obtain interpolation formula for the creep barrier that can be used also at $h \lesssim h_p$. The time scale to overcome this barrier is of the order $\tau(L_h) \approx \tau_0 \exp(\tilde{E}_{B,\text{max}}/T)$, where τ_0 is a microscopic hopping time, which leads to an average velocity,

$$v(h) \approx \gamma h \exp \left[-\frac{T_p}{T} \left(\frac{h_p - h}{h_p} \right)^\theta \left(\frac{h_p}{h} \right)^\mu \right], \quad (8)$$

where γ is the effective friction coefficient [2,3,15,16].

At low temperatures $T \ll T_p$ the dynamic threshold h_p separates the creep regime from the active sliding regime. As can be seen from (8) a characteristic crossover field h_T plays the role of the depinning force, where

$$\frac{h_T}{h_p} = \left(\frac{\tilde{T}_p(h_T)}{T} \right)^{1/\mu} = \left[\frac{T_p}{T} \left(1 - \frac{h_T}{h_p} \right)^\theta \right]^{1/\mu}. \quad (9)$$

At $h \approx h_T$, the drift velocity increases rapidly and at larger fields it displays almost linear behavior $v \approx \gamma h$. Note that h_T is a monotonously decreasing function of temperature with a maximum $h_T = h_p$ at $T = 0$.

In a close vicinity of the threshold field h_p , the effective energy barrier becomes small and even small thermal fluctuations may be sufficient to overcome it. At finite temperatures and $h \lesssim h_p$ the wall moves via thermal activation process with velocity given by Eq. (8). Strictly speaking, it means that at finite temperatures the critical point shifts from $h = h_p$ to $h = 0$. Yet there remains a memory of the critical behavior around $h \approx h_p$ displaying itself in a crossover behavior at finite but low temperatures. The crossover is seen as a *rounding* of the $h - v$ characteristics $v(h \approx h_p) \sim T^{\beta/\theta}$. We now can write an interpolation formula for the velocity which is valid in a wide range of variables:

$$v(h, T) = \gamma h F(x, y); \quad x = h/h_p; \quad y = T_p/T, \quad (10)$$

$$F(x, y) = \frac{\Theta(1-x)}{1 + (yx^{-\mu})^{\beta/\theta}} \exp[-yx^{-\mu}(1-x)^\theta] + \Theta(x-1) \left[\frac{1}{1 + (yx^{-\mu})^{\beta/\theta}} + \left(1 - \frac{1}{x} \right)^\beta \right]. \quad (11)$$

Here $\Theta(x)$ is the step function equal to zero at $x < 0$ and equal to 1 at positive x . The interpolation formula (11) satisfies the following requirements: (i) $v(h, T) = \gamma h$ at any fixed T and $h \gg h_T$; (ii) $v(h, T) = \gamma h \exp[-\frac{T_p}{T} \left(\frac{h_p - h}{h_p} \right)^\theta]$ for $h_p - h \ll h_p$ and $T \ll T_p$; (iii) $v(h, T) \approx \exp[-(T_p/T)(h/h_p - 1)^{-\mu}]$ for $T \ll T_p$, $h \ll h_p$, and $E_{B,\text{max}}/T \gg 1$; (iv) $v(h, T) \approx \gamma h_p (h/h_p - 1)^\beta$ for $(h/h_p - 1) \ll 1$ and $T \ll T_p (h/h_p - 1)^\theta$; (v) $v(h_p, T) \approx \gamma h_p (T/T_p)^{\beta/\theta}$ for $T \ll T_p$.

So far we assumed that the propagating interface is self-affine. This is confirmed by numerical simulations in $D > 1$ interface dimensions for systems with weak disorder [17]. In $D = 1$ dimensions the situation is less transparent: in simulations which use a bounded distribution of random fields the interface appears to be self-affine [18] or faceted [19] depending on whether lattice effects are avoided or admitted, respectively. We ignore here the possibility of faceted growth which occurs only in systems with narrow magnetic domain walls. For an unbounded distribution of random fields, however, a percolative self-similar domain wall propagation was observed [20]. In the following we will always assume that the random fields distribution is bounded such that the domain walls remain well defined. This is also confirmed by our earlier simulation outside of the critical region [10].

Alternating fields.—If the external drive is oscillating with frequency ω , $h = h_0 \sin \omega t$, the barriers for which $\omega \tau(L) > 1$ cannot be overcome during one cycle of the ac field. From the condition $\omega \tau = 1$ we find a *new frequency and temperature dependent* magnetic field h_ω which obeys

$$\frac{h_\omega}{h_p} = \left[\frac{T_p}{T\Lambda} \left(1 - \frac{h_\omega}{h_p} \right)^\theta \right]^{1/\mu}, \quad (12)$$

where $\Lambda = \ln 1/(\omega\tau_0)$. h_ω plays the role of the dynamic threshold. At low fields $h_0 < h_\omega$ there is no macroscopic motion of the wall; its segments oscillate between the metastable states with close energies giving rise to dissipation [2]. Drift of the wall starts at $h_0 > h_\omega$. We assume $\omega\tau_0 \ll 1$, so that $h_\omega < h_T$. Various regimes of domain wall motion are summarized in Fig. 1.

Having derived the domain wall velocity as a function of the driving field in the different h - T regions we consider now the magnetic hysteresis following from the motion of a single wall under the influence of an oscillating field. Since substantial length scales are larger than L_p , where slopes are small, the domain wall will be considered as a straight line (plane) characterized by one coordinate Z [10]. Its dynamics is determined by equation of motion

$$\dot{Z} = v(h(t)). \quad (13)$$

Z varies between limiting values 0 and L . Here L is the linear size of the sample in the case of a single domain wall or, in the multidomain case, equal to the average distance between expanding nuclei. For harmonically oscillating field $h = h_0 \sin \omega t$, Eq. (13) can be rewritten in terms of h only:

$$\frac{dZ}{dh} = \frac{v(h)}{\omega\sqrt{h_0^2 - h^2}}; \quad Z(h=0) = 0. \quad (14)$$

Equations (13) and (14) are valid for $h > h_\omega$. The field region $h < h_\omega$ where the motion has zero drift velocity will not be considered here. The value h_ω plays the role of the threshold field analogous to that of h_p at zero temperature, separating the region with the finite drift velocity from the region where the directed drift is absent. At $h > h_\omega$ the hysteresis is dominated by the activation processes. In this respect it is similar to the nucleation dominated hysteresis described in [10] with two essential differences. First, the activation relates to the formation of a nucleus on the interface, not in the bulk. Second, the activation energy depends on the magnetic field as a power function $\sim h^{-\mu}$

due to the distribution of barriers depending on their length scale.

We start with high temperatures $T > T_p$ where the zero-temperature threshold field h_p plays no role [field sweep (2) in Fig. 1]. In this case the motion of the domain wall is determined by Eq. (14) for $h > h_\omega$. As in the case of zero temperature [10] three dynamic phase transitions take place when the amplitude h_0 increases gradually at a fixed value of frequency. These transitions change the shape (symmetry) of the hysteresis loop. At the first of them proceeding at $h_0 = h_\omega$ the hysteresis loop first appears; at smaller amplitudes $h_0 < h_\omega$ the magnetization remains unchanged. The hysteresis loop appearing at $h_0 > h_\omega$ is characterized by incomplete magnetization reversal and reflection symmetry $h \rightarrow -h, M \rightarrow M$ as shown in Fig. 2a. This symmetry as well as incomplete magnetization reversal persists until the next dynamic phase transition at $h_0 = h_{t1}$.

At $h > h_{t1}$ the magnetization reversal becomes complete and hysteresis loop symmetry changes to inversion $h \rightarrow -h, M \rightarrow -M$ (see Figs. 2b and 2c). The value h_{t1} is determined by a requirement that the domain wall proceeds from one sample boundary to another for half a period. At the next dynamic phase transition the symmetry of the hysteresis loop remains unchanged, but the part of the cycle becomes reversible. Visually the hysteresis loop acquires characteristic “whiskers” as shown in Fig. 2d. The point of this transition h_{t2} is determined by a requirement that the domain wall proceeds from one sample boundary to another for a quarter period.

Starting from the transition amplitude $h_0 = h_{t1}$ each hysteresis loop goes through three important points. One of them is h_ω , at which the motion of domain wall starts, and the two others the so-called coercive field h_c and reversal field h_r . At coercive field the magnetization turns into zero; at reversal field the magnetization becomes completely reversed (see Figs. 2b–2d). Note that, for $h_0 = h_{t1}$, $h_r = h_\omega$ and $h_c = h_0$; for $h_0 = h_{t2}$, $h_r = h_0$. All these fields can be found in our case. Equations for h_{t1} , h_{t2} are

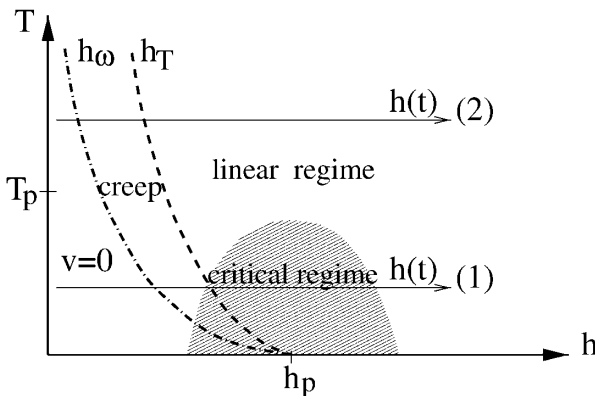


FIG. 1. The phase diagram for the domain wall hysteresis at finite temperature and frequency. Solid and vertical lines separate no sliding, thermal creep, and mechanical drift regimes. See also explanations in the text.

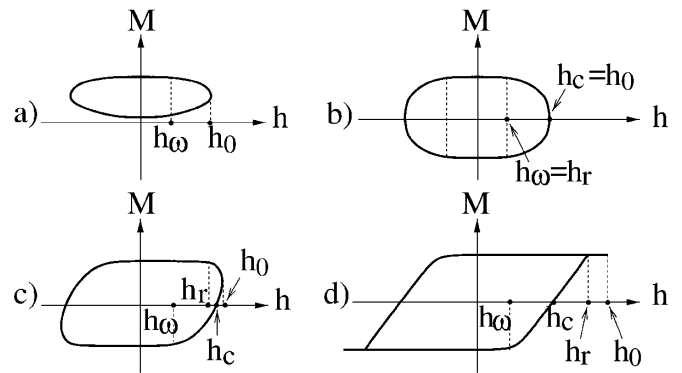


FIG. 2. Schematic pictures of hysteresis loops (HL). (a) Incomplete HL for $h_0 < h_{t1}$. (b) Symmetric HL for $h_0 = h_{t1}$. (c) The HL for $h_{t1} < h_0 < h_{t2}$. (d) The HL for $h_0 > h_{t2}$. The values h_p, h_c, h_r , and h_0 are all marked in all figures.

$$\int_{h_\omega}^{h_m} \frac{v(h) dh}{\sqrt{h_m^2 - h^2}} = \frac{n\omega L}{2}, \quad n = 1, 2. \quad (15)$$

For the case $T > T_p$ Eqs. (15) read

$$g(x_n) = \frac{n\omega L}{2\gamma h_T}, \quad g(x) = \int_{x_\omega}^x y e^{-y^{-\mu}} (x^2 - y^2)^{-1/2} dx, \quad (16)$$

where $x_n = h_{in}/h_T$, $n = 1, 2$; $x_\omega = h_\omega/h_T = 1/\Lambda^{1/\mu}$. Thus, x_1, x_2 are functions of a dimensionless parameter $u = \omega L/\gamma h_T$, where L is the size of the system or an average size of domains. Its asymptotic at small u results in $x_n \approx [\ln(2/nu)]^{-1/\mu}$. The fields h_{t1}, h_{t2} are close in this case: $(h_{t2} - h_{t1})/h_{t1} \approx \ln 2/(\mu \ln u)$. The requirement $h_{t1} > h_\omega$ is satisfied if $\gamma h_T \tau_0 < L$. The coercive field h_c and the reversal field h_r are determined by equations $M(h_c) = 0$; $|M(h_r)| = M_s$. A simple analysis at small u results in $h_c \approx h_{t1}$; $h_r \approx h_{t2}$. The area \mathcal{A} of the hysteresis loop at $u \ll 1$ and $h_0 > h_{t1}$ does not depend strongly on the amplitude h_0 . Figure 2 represents typical shapes of hysteresis loops and illustrates the geometrical meaning of the field h_ω, h_c, h_r . It is approximately $\mathcal{A} \approx 4h_r M_s$. The dependence of magnetization on magnetic field is given by equation $M(h) = M_s(\frac{2Z(h)}{L} - 1)$.

Finally, in the range of moderately low temperatures $T < T_p$ the more complete expressions (10) and (11) have to be used in integrating Eq. (14).

It is interesting to note that the similar (dynamic) transition from incomplete to complete hysteresis was observed even in a standard simplistic mean-field model for pure magnets with the reaction described by the Brillouin function [21]. This suggests that this kind of dynamic transition which we discuss may be a generic property of nonlinear systems. Another note is in order: hysteresis in large multidomain magnet samples is a very complex phenomenon and cannot always be reduced to motion of a single domain wall (see, for example, numerical simulations of random Ising model in [22], where hysteretic and memory effects unlikely reducible to motion of a single DW were revealed).

In conclusion, we have investigated critical creep motion at low, $T \ll T_p$, and at high, $T > T_p$, temperatures, T_p being the depinning temperature, and constructed the dynamic phase diagram. At low temperatures creep at $h \approx h_p$ retains features of the critical behavior and exhibits the rounding of the $h - v$ characteristic, according to [13]. At finite frequencies ω , a new characteristic field $h_\omega < h_p$ comes into play, and the transition from the sliding regime to pinning dominated activation motion is shifted to h_ω .

We are grateful to A. Middleton for a valuable discussion. One of us (V.P.) acknowledges the support of this work by the NSF under Grants No. DMR-97-05182 and No. DMR-00-72115 and by the DOE under the Grant

No. DE-FG03-96ER45598, as well as from the Humboldt Foundation. The work at ANL was supported by the U.S. DOE, Office of Science under Contract No. W-31-109-ENG-38.

- [1] For recent reviews see, e.g., M. Kardar, Phys. Rep. **301**, 85 (1998); D. S. Fisher, Phys. Rep. **301**, 113 (1998).
- [2] L. B. Ioffe and V. M. Vinokur, J. Phys. C **20**, 6149 (1987).
- [3] T. Nattermann, Phys. Rev. Lett. **64**, 2454 (1990).
- [4] M. V. Feigelman, D. B. Geshkenbein, A. I. Larkin, and V. M. Vinokur, Phys. Rev. Lett. **63**, 2303 (1989).
- [5] G. Blatter, M. V. Feigelman, V. B. Geshkenbein, A. I. Larkin, and V. M. Vinokur, Rev. Mod. Phys. **66**, 1125 (1998).
- [6] D. S. Fisher, Phys. Rev. Lett. **50**, 1486 (1983).
- [7] O. Narayan and D. S. Fisher, Phys. Rev. B **46**, 11 520 (1992).
- [8] T. Nattermann, S. Stepanow, L. H. Tang, and H. Leschhorn, J. Phys. II (France) **2**, 1483 (1992).
- [9] O. Narayan and D. S. Fisher, Phys. Rev. B **48**, 7030 (1993).
- [10] I. F. Lyuksyutov, T. Nattermann, and V. L. Pokrovsky, Phys. Rev. B **59**, 4260 (1999).
- [11] T. Halpin-Healy and Y-C. Zhang, Phys. Rep. **254**, 215 (1995).
- [12] D. S. Fisher, Phys. Rev. Lett. **56**, 1964 (1986).
- [13] A. Middleton, Phys. Rev. Lett. **68**, 670 (1992).
- [14] At $T = 0$ pinning potential acquires a ratchet-kick shape at large distances for which $\theta = 2$ [13]. However, at finite temperatures the smearing occurs at $L \approx L_p$, and the system may not have enough "time" to generate the "ratchet-kick" potential. Since θ is nonuniversal we do not specify its value.
- [15] For a RG derivation of 8 see L. Radzihovsky, APS March Meeting 1998, and P. Chauve, T. Giamarchi, and P. Le Doussal, Europhys. Lett. **44**, 110 (1998).
- [16] For completeness we note here that equilibrium RF systems in $d = D + 1 = 2$ bulk dimensions have no long range order at length scales $L \gg \xi_{RF} \approx l \exp(\Gamma/v)^{4/3}$ [see J. Villain, J. Phys. (Paris), Lett. **43**, L551 (1982); G. Grinstein and S.-K. Ma, Phys. Rev. Lett. **49**, 685 (1982)]. For weak disorder ξ_{RF} is very large and can easily exceed the system size. As soon as an external field is applied such that $L_h < \xi_{RF}$, domain wall motion is dominated by the forces on scales L_h and the absence of true long range order can be ignored.
- [17] L. Roters, A. Hucht, S. Lubeck, U. Nowak, and K. D. Usadel, Phys. Rev. E **60**, 5202 (1999); B. Koiller and M. O. Robbins, arXiv:cond-mat/0004183, and references therein.
- [18] U. Nowak and K. D. Usadel, Europhys. Lett. **44**, 634 (1998).
- [19] H. Ji and M. O. Robbins, Phys. Rev. B **46**, 14 519 (1992).
- [20] B. Drossel and K. Dahmen, Eur. Phys. J. B **3**, 485 (1998).
- [21] B. K. Chakrabarti and M. Acharyya, Rev. Mod. Phys. **71**, 847 (1999).
- [22] J. P. Sethna, K. Dahmen, S. Kartha, J. A. Krumhansl, B. W. Roberts, and J. D. Shore, Phys. Rev. Lett. **70**, 3347 (1993); K. Dahmen and J. P. Sethna, Phys. Rev. Lett. **71**, 3222 (1993).